Journal of Nuclear Materials 424 (2012) 158–163

Contents lists available at SciVerse ScienceDirect

Journal of Nuclear Materials

journal homepage: www.elsevier.com/locate/jnucmat

Many-body interatomic U and Al–U potentials

M.I. Pascuet [a,*], G. Bonny [b], J.R. Fernández [a,c]

[a] CONICET, Avda. Rivadavia 1917, 1033 Buenos Aires, Argentina
[b] SCK·CEN, Studiecentrum voor Kernenergie·Centre d'Etude de l'Energie Nucléaire Boeretang 200, 2400 Mol, Belgium
[c] CNEA, Gral. Paz 1499, 1650 San Martin, Buenos Aires, Argentina

ARTICLE INFO

Article history:
Received 28 December 2010
Accepted 2 March 2012
Available online 9 March 2012

ABSTRACT

In the present work, an interatomic potential in the framework of the embedded atom method (EAM) is developed for the Al–U binary system. A methodology is detailed to fit the U potential, that reproduces the stability of the α phase at low temperatures and the γ phase at high ones. The thermal stability of both phases, thermal expansion and vacancy driven self diffusion are studied. The Al–U potential is fit to first principles calculated formation energies of the experimentally observed intermetallic phases, Al_2U (cubic C15), Al_3U (cubic $L1_2$) and Al_4U (orthorhombic $D1_b$). As a first validation the potentials are tested against available experimental measurements.

1. Introduction

In recent years, aluminum-based alloys containing U–Mo in gamma phase are proposed as the new nuclear fuels for research and test reactors. These fuel elements allow fulfillment of requirements to use low enriched U [1–3].

A dispersion fuel element consists of a "meat" by mixture of powders of an U(Mo) alloy and Al, cladded with an Al alloy. During the fabrication and/or irradiation the fuel particles react with the surrounding Al matrix. Post-irradiation experiments have shown a significant interaction layer producing a considerable swelling and unacceptable porosity [4]. This interaction layer is formed by new phases whose composition ranges between those of the limiting components, and is responsible for changes in the specific volume and in the thermomechanical properties [5,6].

Predicting these effects that degrade the material, requires knowledge of phenomena operating at the atomic level, which are difficult to access by experiment. In recent years atomistic simulation methods are becoming increasingly important as a tool in support of experiments, since they are able to separate the effects of various components of the evolution of the microstructure and thus reveal fundamental physical mechanisms of degradation. First principles methods have proven to be very accurate tools in describing various material properties, but are only applicable to a small-scale atomic system. To overcome this limitation, atomic interactions are described by many-body central-force potentials, in particular the "embedded atom method" (EAM) [7] which is widely used to describe metals and their alloys. Qian et al. [8] have built a Morse potential for the UCu_5TAl_6 (T = Cr, Mn and Fe) intermetallics to calculate structure and thermodynamic properties. This potential, however, is not appropriate for simulations in the Al–U system because, for example, the pure metals are not described properly. It is very desirable that an interatomic potential is able to reproduce as closely as possible the stability of the phases that can appear at least in the concentration range of interest.

Pure U undergoes different allotropic transformations as temperature increases. At low temperatures the α phase (*strukturbericht* A20) is stable for $T < 940$ K. It consists of a *c*-face centered orthorhombic structure with two atoms per primitive cell at positions $(\pm y, \mp y, \mp 1/4)$, expressed in units of the primitive vectors $(a/2, -b/2, 0)$, $(a/2, b/2, 0)$ and $(0, 0, c)$, as illustrated in Fig. 1. At intermediate temperatures ($940\ \text{K} < T < 1045\ \text{K}$) the β phase occurs, which has a complex tetragonal structure containing 30 atoms per unit cell (A_b) [9]. Finally, the bcc γ phase (A2) is stable up to the melting point ($T_m = 1405$ K).

Regarding the Al–U binary alloy, a re-evaluation of the phase diagram made by Kassner et al. [5] shows the formation of three low temperature intermetallic phases: Al_2U, a cubic C15 Laves phase; Al_3U, cubic of type $L1_2$; and Al_4U, orthorhombic of type $D1_b$. The authors treat these phases as line compounds with the exception of Al_4U, for which a polymorphic transformation has been considered to occur at 919 K due to rearrangement of constitutive vacancies. In view of the newer results of Tougait and Noël [10] for Al_4U, all three intermetallics will here be considered as stoichiometric compounds.

In the present work, interatomic many-body potentials of EAM-type for the Al–U binary system are developed. Section 2 recalls the EAM formalism and describes the fitting methodology. In Section 3

* Corresponding author. Tel.: +54 11 6772 7254; fax: +54 11 6772 7303.
E-mail address: pascuet@cnea.gov.ar (M.I. Pascuet).

0022-3115/$ - see front matter © 2012 Elsevier B.V. All rights reserved.
http://dx.doi.org/10.1016/j.jnucmat.2012.03.002

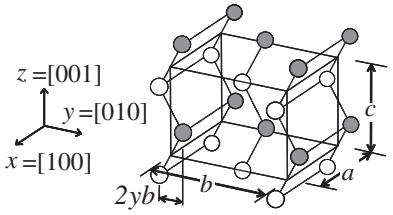

Fig. 1. Orthorhombic unit cell and lattice parameters in αU.

the potential's performance is assessed by calculating different properties which are compared with available results from the literature. The paper is finalized by a discussion about the range of applicability of the potential.

2. Potential formalism and fitting procedure

In the EAM framework, the total energy is a sum of atomic/site contributions, expressed as [7],

$$E_i = \frac{1}{2}\sum_{j\neq i} V(t_i t_j; r_{ij}) + F(t_i; \rho_i), \tag{1}$$

where $t_i(t_j)$ stands for the chemical species at the site $i(j)$, V is the pair potential, r_{ij} is the distance between atoms i and j, and F is the so called "embedding function". The local electron density ρ_i at site i in turn results from the superposition of electronic potentials, ϕ, given as,

$$\rho_i = \sum_{j\neq i} \phi(t_i t_j; r_{ij}). \tag{2}$$

To fully describe all interactions in the Al–U binary system, the following seven functions are needed: V_{Al}, V_U, ϕ_{Al}, ϕ_U, F_{Al} and F_U, which correspond to interactions in the pure elements, and the cross potential V_{AlU}. The pure Al potential developed by Zope and Mishin [11] is used in this work, which reproduces the experimentally observed lattice parameters, cohesive energy, elastic constants, stability of fcc lattice against other simple structures, and vacancy formation and migration energies. The pure U potential and Al–U cross interaction on the other hand are developed in the present work.

The pair potentials for V_U and V_{AlU} are expressed as a piecewise cubic spline of the form,

$$V(r) = \sum_{k=1}^{m} A_k (r - R_k)^3 H(R_k - r), \tag{3}$$

where H is the Heaviside unit step function, R_k are the knot points and A_k the fitting coefficients. The electronic density ϕ_U is chosen as the Thomas–Fermi screening function, smoothly matched to zero at the cut off range,

$$\phi(\chi) = \begin{cases} e^{-\beta\chi}/\chi & \chi \leqslant \chi_1 \\ (\chi - \chi_2)(h_1\chi^2 + h_2\chi + h_3) & \chi_1 \leqslant \chi \leqslant \chi_2, \\ 0 & \chi_2 \leqslant \chi \end{cases} \tag{4}$$

Table 2
Embedding function F_U (eV) for pure uranium (ρ_0 is the equilibrium electron density).

ρ/ρ_0	$F_U(\rho)$	ρ/ρ_0	$F_U(\rho)$
0.1190000	−2.4167961500	1.1533390	−4.3714970334
0.1348548	−2.5729759879	1.2776855	−4.3119240988
0.1526138	−2.7084626124	1.4141300	−4.2130266732
0.1724811	−2.8203485935	1.5637241	−4.0692865503
0.1946800	−2.9264460029	1.7276000	−3.8748425732
0.2194549	−3.0408691210	1.9069757	−3.6230940042
0.2470725	−3.1646882471	2.1031613	−3.3039896933
0.2778241	−3.2965407012	2.3175643	−2.9048866720
0.3120271	−3.4348807875	2.5516962	−2.4136512582
0.3500274	−3.5778867660	2.8071792	−1.8007480135
0.3922015	−3.7233857207	3.0857533	−1.0346501921
0.4389586	−3.8663495600	3.3892835	−0.1242394267
0.4907434	−3.9947098947	3.7197678	0.9099228254
0.5480388	−4.0993027890	4.0793453	2.0697281153
0.6113684	−4.1851315237	4.4703050	3.3686297584
0.6812997	−4.2589671080	4.8950949	4.8229243450
0.7584475	−4.3208380330	5.3563314	6.4418219341
0.8434768	−4.3672273121	5.8568095	8.2260257695
0.9371067	−4.3941422056	6.3995134	10.1985264864
1.0401144	−4.3971689958	6.9876277	12.3979426971

where $\chi = r/a_0$ and a_0 the equilibrium lattice parameter of αU phase along the [1 0 0] direction (see Fig. 1). The values for the parameters β, χ_1, χ_2, h_1, h_2 and h_3 are given in Table 1. The embedding function on the other hand has no analytic function, but a tabulation containing knot points for cubic interpolation is provided (Table 2).

The potential for pure U is fitted to reproduce as close as possible the lattice parameters, cohesive energy, bulk modulus, and vacancy formation and migration energies corresponding to orthorhombic αU. It has been found that $m = 3$ in Eq. (3) is the minimum value that satisfies the constraints deduced from all these properties.

Firstly, equilibrium lattice parameters impose null atomic forces and stresses on the orthorhombic unit cell. Without loss of generality $F(\rho)$ is imposed to have null first derivative at the equilibrium lattice density, $F'(\rho_0) = 0$, which makes $V(r)$ an "effective pair potential" [11]. Taking this into account, the null atomic force condition on a generic atom 0 is expressed as,

$$\sum_{k=1}^{3} A_k \left[\sum_v \frac{(R_k - r_v)^2}{r_v} H(R_k - r_v) \left(\sum_{j\in v} x_{0j} \right) \right] = 0, \tag{5}$$

here x_{0j} is the $x \equiv [1\,0\,0]$ component of the position vector $\mathbf{r}_{0j}$ from a reference atom 0 to atom j, and the sum in square brackets extends over all neighbor shells v around the reference atom. Similar expressions hold for $y \equiv [0\,1\,0]$ and $z \equiv [0\,0\,1]$ directions. Due to mirror symmetries of the αU lattice, all conditions are identically zero except for the one corresponding to the [0 1 0] direction. Regarding null stresses, only normal components survive due to the same lattice symmetries, so that the next must hold for the x direction,

$$\sum_{k=1}^{3} A_k \left[\sum_v \frac{(R_k - r_v)^2}{r_v} H(R_k - r_v) \sum_{j\in v} x_{0j}^2 \right] = 0. \tag{6}$$

Table 1
Optimized parameters R_k (Å), A_k (eV/Å^3) and F_0'' (eV) for the pair potentials V_U and V_{AlU} and β, χ_i, h_i for electronic density ϕ_U.

Potential parameters for pure U				Potential parameters for Al–U			
R_1	4.50	β	5.0	R_1	6.0	A_1	−0.01126
R_2	4.35	χ_1	1.75	R_2	3.5	A_2	0.62769
R_3	4.20	χ_2	2.1				
A_1	−2.6217703	h_1	−0.035708982				
A_2	5.5043693	h_2	0.118645639				
A_3	−2.8225308	h_3	−0.100383042				
F_0''	2.4692407						

Table 3
Number of atoms n_v and distance r_v for each shell v in a perfect αU lattice.

Shell v	n_v	r_v^2
1	2	$(2yb)^2 + (c/2)^2$
2	2	a^2
3	4	$(a/2)^2 + (b/2)^2$
4	4	$(a/2)^2 + (b/2 - 2yb)^2 + (c/2)^2$
5	4	$a^2 + (2yb)^2 + (c/2)^2$
6	2	c^2

Similar expressions are obtained for y and z directions. If in addition the knot values R_k are all restricted to lie between fifth and sixth neighbor distances, $r_5 < R_k < r_6$, and the first and second as well as the third and fourth neighbor distances are forced to be equal, i.e., $r_1 = r_2$ and $r_3 = r_4$ (see Table 3), then, the following relationships hold for the lattice parameters,

$$\frac{b}{a} = \frac{1}{\sqrt{2y}}; \quad \frac{c}{a} = 2\sqrt{1-2y}. \tag{7}$$

In this case, all Eq. (6) are linearly dependent and only one of the three equations remain. Although these assumptions may sound very restrictive, they allow a reasonable short-range interaction with the fewest number of adjustable parameters.

Secondly, cohesive energy and bulk modulus are imposed by forcing the embedding function F to reproduce Rose's universal equation of state [12], in a similar way as explained in [13,14]. The value of the cohesive energy has been estimated adding up first principles results for the cohesive energy of the γ phase [15] and the energy difference between γ and α [16], giving $E_c = 5.773$ eV. This value compares reasonably well with the experimental one, 5.55 eV [17].

Thirdly, the unrelaxed vacancy formation energy is fitted (estimated as $E^f_{UR} = 1.4$ eV). If no lattice relaxation is allowed, this energy results [14]:

$$E^f_{UR} \approx -\frac{1}{2}\sum_v n_v[V(r_v) - F_0''\phi^2(r_v)], \tag{8}$$

where n_v is the number of atoms in neighbor shell v and $F_0'' = d^2F/d\rho^2$ is evaluated at the equilibrium lattice density. By substituting Eq. (3), this condition becomes

$$\sum_{k=1}^{3} A_k \left[\sum_v n_v (R_k - r_v)^3 H(R_k - r_v)\right] = \sum_v n_v \phi^2(r_v) F_0'' - 2E^f_{UR}. \tag{9}$$

Eqs. (5), (6), and (9) form a set of three equations in the three unknowns A_k. It should be noted that this set is not linear in A_k, since F_0'' in Eq. (9) depends implicitly on A_k. To solve it, the system is first linearized by taking an initial guess for the values of A_k from which F_0'' can be calculated. Then the problem is solved iteratively until the difference between successive values of A_k are less than 10^{-7} eV/Å^3.

Lattice stability against other simple lattices, like simple hexagonal, hcp, bcc and fcc, is possible by choosing appropriate values of R_k and by playing with the balance between the fully relaxed vacancy formation and migration energies E^f and E^m (taking into account that the only experimental magnitude known is the activation energy $Q = E^f + E^m$) [18,19].

The optimized potential parameters resulting for pure U from the above procedure are reported in Table 1. The embedding function $F(\rho)$ is tabulated in 40 non-equidistant points and tabulated in Table 2. A cubic spline interpolation through these points gives $F(\rho)$ with an error of at most 10^{-3} eV. Tables containing more points for these potentials are available on-line [20].

The presently fitted pure U potential and the Al potential – taken from Zope and Mishin [11] – are combined to determine the cross interaction for the Al–U system. This requires the V_{AlU} cross potential and the scaling factor between the equilibrium electronic densities ρ_{Al}/ρ_U [11] to be fitted. The latter relationship is estimated from the work of Miedema [21] as $\rho_{Al}/\rho_U = 2$. For the V_{AlU} potential a similar functional form as in Eq. (3) is chosen. In this case, the new fitting parameters A_k are optimized by minimizing an objective function,

$$S(A_k) = \sum_{i=1}^{3} (\Delta E^f_{0i} - \Delta E^f_i)^2, \tag{10}$$

where the sum i extends over the three experimentally observed low temperature intermetallic compounds (see Section 1), ΔE^f_{0i} and ΔE^f_i are the reference and calculated formation energies of compound i, respectively. The minimization of S is performed under the constraints of minimum stresses in each of the considered compounds. First principles values of lattice parameters and formation energies [22] are used to fit the potential parameters. It was found that the minimization of S can be achieved by taking $m = 2$ in Eq. (3). The optimized parameters describing the cross potential are summarized in Table 1.

3. Results and discussion

3.1. Pure U

Table 4 summarizes the lattice parameters for αU obtained with the present interatomic potential. They are in reasonable agreement with both first principles [16] and experimental values [16,23].

The thermal behavior of the experimentally observed phases is also studied. Molecular dynamics (MD) simulations of a cubic box

Table 4
Calculated, first principles [16], and experimental values of lattice parameters, atomic volume and energy differences between fcc, bcc, hcp and αU.

	EAM (this work)	F.P.	Exp
a (Å)	2.775	2.845	2.836[a]
b (Å)	6.072	5.818	5.866[a]
c (Å)	4.936	4.996	4.935[a]
y	0.1044	0.1025	0.1017[a]
$\Delta E_{fcc\text{-}\alpha}$ (eV)	0.169	0.260	0.052[b]
$\Delta E_{bcc\text{-}\alpha}$ (eV)	0.007	0.223	0.079[b]
$\Delta E_{hcp\text{-}\alpha}$ (eV)	0.169	0.241	0.131[b]

[a] Ref [16].
[b] Extrapolated to low temperatures from [23].

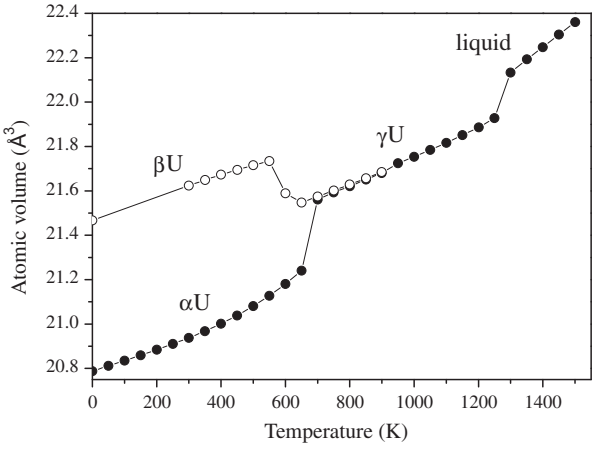

Fig. 2. Atomic volume Ω as a function of temperature T. Full (empty) symbols correspond to MD results in which αU (βU) lattice is the starting structure.

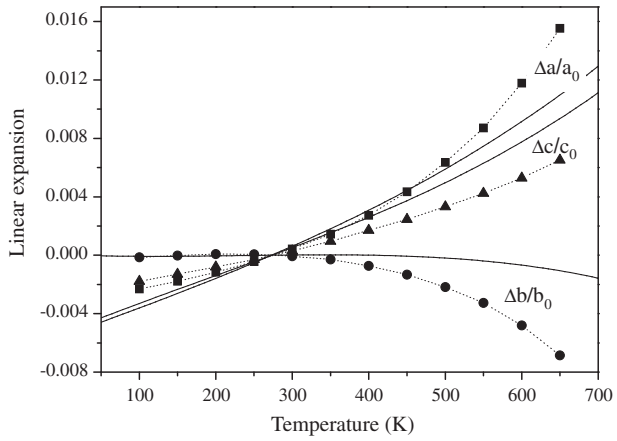

Fig. 3. Linear expansions along *a*, *b*, *c* for the orthorhombic cell in αU as a function of temperature. Dashed lines and symbols show results of the present work and solid lines indicate experimental results [24]. a_0, b_0, and c_0 are the reference values at 273 K.

composed of $9 \times 4 \times 5$ orthorhombic unit cells ($N = 720$ atoms) are performed in (N,P,T) ensemble in the range $0 < T < 1500$ K and $P = 0$ Pa in steps of 50 K, starting from equilibrium atomic positions at 0 K. Periodic boundary conditions are chosen for all simulation. The average atomic volume resulting from the simulations is plotted as a function of temperature in Fig. 2. Two discontinuities are observed at ~650 K and 1250 K corresponding to phase transitions, which are identified as the αU → γU and γU → U(liquid) transitions. As βU is not observed with this procedure, it is simulated separately starting from its ideal tetragonal structure at 0 K [9]. The results show that the βU structure is metastable from 0 to 550 K and then transforms into γU. Despite the fact that these transformations occur at much lower temperatures than observed in experiment, it is striking that a relatively simple EAM potential is able to capture this non-trivial temperature behavior.

From the same set of simulations it is possible to calculate the thermal linear expansion coefficients of αU, shown in Fig. 3. It is seen that, while the lattice expands in the [100] and [001] directions, there is an anomalous lattice contraction along the [010] direction, in general agreement with experimental results [24,25].

Next, the vacancy's static and dynamic properties are studied. Its formation energy and jump barriers to nearest positions are calculated at 0 K by means of molecular statics (MS), using the same simulation crystal already described. The vacancy formation energy is then defined as,

$$E^f = E_{DL} - E_{PL} - E_c, \tag{11}$$

where E_{DL} is the energy of the lattice with $N - 1$ atoms and the vacancy, E_{PL} the energy of the perfect lattice with N atoms, and E_c is the cohesive energy. After full relaxation of the atomic forces, the resultant value is $E^f = 1.36$ eV. The temperature dependence of E^f is then studied using MD. In this case, an atom is extracted from a crystal of the same size used in our previous bulk studies and run for the same temperatures and under the same simulation conditions. The two simulation sets, with and without defect, allow to use a similar expression as in Eq. (11) to calculate the vacancy formation energy at each temperature. A clear temperature behavior could not be established due to the large scatter. Therefore we only report the average values for both αU (1.4 ± 0.2 eV) and γU (1.7 ± 0.9 eV) phases. From first principles calculations, Taylor [26] have obtained 1.95 eV and Beeler et al. [27] 1.86 eV for αU. Using the same computation technique, Xiang et al. [28] have obtained 1.08 eV and Beeler et al. 1.32–1.38 eV [27] for γU. From positron annihilation spectroscopy, Matter et al. [29] have measured 1.2 ± 0.25 eV for γU.

Energy barriers for jumps to nearest lattice positions in αU are calculated using the drag method [30] under the same simulation conditions. Values obtained for these jumps are depicted in Fig. 4. The two lowest values correspond to vacancy movements along [100] and the zig-zag [001] directions while higher values are obtained for jumps lying mainly along [010].

The values of the energy barriers obtained by MS are introduced as an input into a kinetic Monte Carlo (MC) code to calculate the diffusivity in αU [31]. In MC simulations, atoms are located in a rigid lattice and the system evolves through exchanges between atoms and a vacancy, simulating diffusion processes [32]. The energy barriers for the vacancy jumps are used to assess the jump probability and choose the event according to the Metropolis [33] scheme, thereby setting the rate of time employing the residence time algorithm [34]. Calculations are made by assuming all attempt frequencies are equal to the Debye frequency (10^{13} s^{-1}). Averages are taken from one hundred different simulations at each temperature in the range $400\ \text{K} \leqslant T \leqslant 600$ K.

For comparison, MD simulations in a crystal box of similar size are also performed for the same temperature range. After equilibration at each temperature in the (N,P,T) ensemble for 100 ps, mean square displacements are calculated by running in the (N,V,E) ensemble for 60 ns. Fig. 5 compares the obtained results for both MC and MD techniques in an Arrhenius plot. The results show that the diffusion is faster in the [100] direction compared

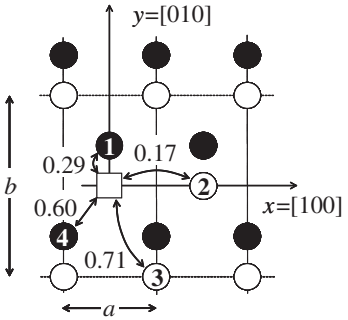

Fig. 4. Jump energy barriers (in eV) for αU. Empty (full) circles are atoms in $z = 0$ ($z = c/2$) and the square denotes the vacancy. Numbers inside the circles indicate the nearest neighbor shell.

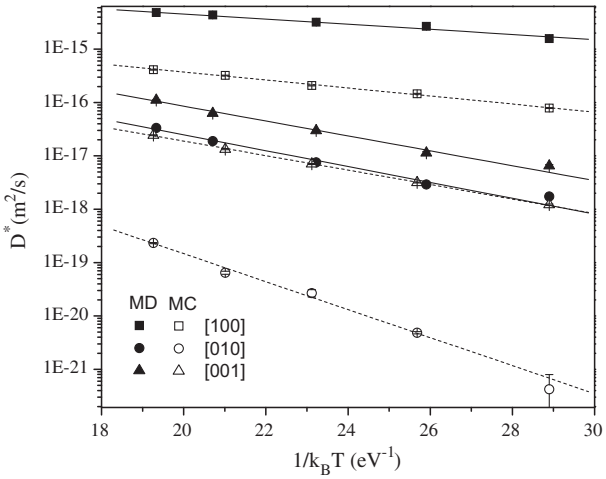

Fig. 5. Diffusion coefficients D^* by vacancy mechanism as a function of temperature in αU obtained by MC and MD simulations.

Table 5
Migration E^m and activation $Q = E^f + E^m$ energies obtained by MD and MC. Experimental values are reported in parentheses.

Phase	Direction	E^m (eV)		Q (eV)	
		MD	MC	MD	MC
Uα	[100]	0.11	0.17	1.51	1.53
	[010]	0.34	0.60	1.74	1.96
	[001]	0.32	0.31	1.72 (1.74–1.91[a])	1.67
Uγ		0.68	–	2.38 (1.15–1.24[a])	–

[a] Ref. [19].

to the [010] and [001] directions. The apparent disagreement between MC and MD techniques can be partly attributed to an effect of the attempt frequency used: while MD simulations implicitly take into account the full influence of cooperative jumps, MC assumes that the attempt frequency is constant.

These results are in agreement with the vacancy diffusion model proposed by Seigle and Opinsky [35]. They proposed that self-diffusion by vacancies in αU should be essentially anisotropic, because the jump frequencies should be higher for neighbors lying on the corrugated (010) planes, where covalent bonds are stronger. Thus, one should expect a much lower diffusion coefficient along the [010] direction compared to the other orthogonal directions. Resnick and Seigle [36] did not find large diffusion anisotropy in single crystals at 913 K, although they acknowledged that the radiographic technique used had poor accuracy. On the other hand, Rothman et al. [37,38] found that $D_{[100]} \approx D_{[001]} \gg D_{[010]}$ using the sectioning method.

Diffusivity by vacancy mechanism is also obtained for γU using the MD technique for a simulation box of approximately the same size for the temperature range 800 K $\leqslant T \leqslant$ 1200 K under the same simulation conditions. As the bcc lattice is unstable under the presence of a vacancy at $T = 0$ K, it was not possible to obtain an energy barrier for the vacancy jump in γU by using the MS technique and, therefore, no MC simulations were done.

From the diffusivity, migration energies are obtained as, $D^* = D_0^* \exp(-E^m/kT)$. Table 5 compares the activation energies for both simulation techniques, calculated as $Q = E^f + E^m$, and experiment. The obtained values are in rather good agreement with the self diffusion activation energies reported in the literature for αU but are overestimated for the case of γU [19].

3.2. Al–U

The formation energies and lattice parameters of the intermetallics obtained with the potential are shown in Table 6 and compared to first principles and experimental values. It is worth to note that the obtained formation energies, as well as the fitted first principles values, fall short of the experimental values.

Table 6
Calculated, first principles (italic) [22], and experimental (parentheses) values of lattice parameters and formation energies for intermetallics.

Phase	a (Å)	b (Å)	c (Å)	ΔE_0^f (eV/at.)
UAl_2 (C15)	7.585 *7.635* (7.760[a])	–	–	−0.115 *−0.127* (−0.319 ± 0.03[a])
UAl_3 ($L1_2$)	4.166 *4.238* (4.265[a])	–	–	−0.104 *−0.096* (−0.281 ± 0.03[a])
UAl_4 ($D1_b$)	4.128 *4.356* (4.410[a])	6.470 *6.197* (6.270[a])	13.691 *13.671* (13.710[a])	−0.038 *−0.039* (−0.258 ± 0.03[a])

[a] Ref. [5].

The elastic properties for each intermetallic structure are calculated by using the MS technique, taking into account relaxation of internal atomic coordinates. Table 7 reports the obtained values of bulk modulus B and its derivative with respect to pressure B'. It is seen that the predicted values of B are in rather good agreement to first principles values but somewhat in excess from experimental ones, although they seem to show a large scattering [39,40].

Next, MD simulations of bulk Al with U impurities are made to calculate the mobility of the different species at different temperatures. A simulation box of $5 \times 5 \times 5$ fcc cubic cells containing $N = 500$ Al atoms is used and then one Al atom is picked at random and extracted to generate a vacancy. Subsequently, five U substitutional atoms are added at random positions so as to reach ∼1%at.U composition. As mentioned above in the case of αU vacancy diffusion, the configurations are thermalized for 100 ps under zero pressure in (N,P,T) ensemble. The temperatures are chosen in the range 600 K $\leqslant T \leqslant$ 850 K. The output configuration from each equilibration run is subsequently used for longer runs of 6 ns in (N,V,E) ensemble, in which the mobility D^* is calculated through mean square displacements of each species. Similar simulations are performed in a U–1%at.Al system by adding a vacancy and 7 Al atoms to the block of $N = 720$ U atoms but in a lower temperature range, 400 K $\leqslant T \leqslant$ 600 K. As shown in Fig. 6, the U diffusivity is faster in Al than viceversa.

Present diffusivity results are obtained in dilute alloys and they are not directly comparable to experimental values from the literature, which are based on measurements on diffusion couples [41]. On the other hand, experimental results are somewhat controversial and difficult to assess due to phase decomposition and formation of intermetallics. Diffusion couples have been studied by a number of authors [42–47]. Most of them observe the formation of Al_3U only. The reason for this could be attributed to the slower growth kinetics of Al_2U and Al_4U as compared to that of Al_3U [48]. In diffusion couples of Al and stabilized γ(U,Mo) alloys, Mirandou et al. [49] show that when there is no γU → αU decomposition the interface is smooth and uniform and no Al is detected into the γ phase. When decomposition takes place, the width of the interaction layer increases and the interface is irregular on the U end, attributed to a faster growth rate of Al_3U into αU. There seems to be some controversy in the literature regarding the fastest diffuser. Le Claire and Bear [50] performed diffusion experiments in Al/U

Table 7
Calculated, first principles (italic) [22], and experimental (parenthesis) values for the bulk modulus B and its pressure derivative B' for each of the pure elements and intermetallics in the Al–U system.

	B (GPa)	B'
Al	79 *78* (75.2[a])	4.10
U	132 *136* (133–135.5[a])	4.46
Al_2U	117 *111* (82.39 ± 8.99[b])	4.22 (9.29 ± 3.55 [b])
Al_3U	112 *94* (66.55 ± 6.65 [b])	3.90 (12.58 ± 2.48 [b])
Al_4U	76 *94* (71.35 ± 4.77 [b])	3.01 (6.60 ± 0.80 [b])

[a] Ref. [17].
[b] Ref. [39].

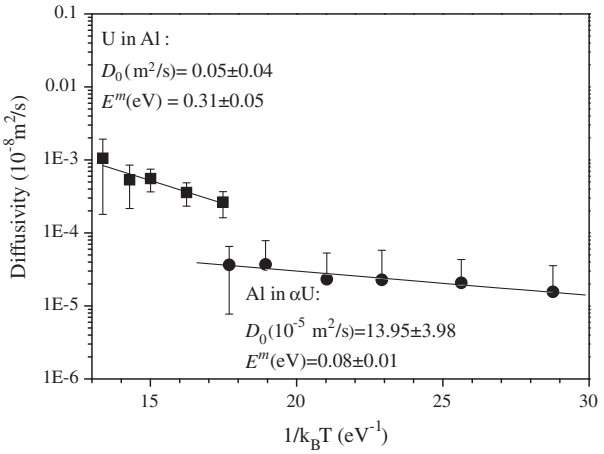

Fig. 6. Arrhenius plot of the diffusivity of U into Al–1%at.U and Al into U–1%at.Al.

couples and found that U penetrates deeper into Al 2.25 times faster than Al into U. Perez et al. [51] have studied diffusion couples of U–Mo vs. Al and Al–Si and suggest that the formation of intermetallics in the diffusion layer requires that Al diffuses intrinsically much faster than the other species. More experimental research is needed to shed some light into these problems.

4. Concluding remarks

In the present work, an EAM interatomic potential has been developed to model Al–U alloys. First, pure U potential has been obtained following the methodology explained. It reproduces the stability of orthorhombic αU at low temperatures and the transformation to bcc γU at higher temperatures, as observed experimentally. Thermal behavior, thermal linear expansion and vacancy properties are in agreement with experiments. The atomic transport, predicted by the present simulations, shows faster diffusivity along the [100] and [001] axis than along [010] with some differences depending on the simulation technique used. The obtained activation energies show good agreement with the experimental values for αU, and a clear overestimation for γU. These results suggest that only the qualitative behavior of the metal can be studied at high temperatures with the present potential.

Regarding Al–U alloys, the cross potential has been fitted taking into account the available first principles data. Lattice parameters, formation energies and bulk modulus for each intermetallic compound are reasonably well reproduced. Simulations on dilute alloys suggest a faster diffusivity of U in Al than viseversa. More detailed studies are being performed to take into account the role of intermetallics in the interdiffusion process.

Acknowledgements

This research was partially supported by PIP 5062 (CONICET), PIP 804/10 (CONICET), C057 (UNSAM) and FW/09/03 (MINCyT-FWO bilateral cooperation agreement, Argentina–Belgium). The authors would like to thank Dr. R.C. Pasianot for fruitful discussions.

References

[1] J. Snelgrove, G. Hofman, M. Meyer, C. Trybus, T. Wiencek, Nucl. Eng. Des. 178 (1997) 119.
[2] M.K. Meyer, G.L. Hofman, S.L. Hayes, C.R. Clark, T.C. Wiencek, J.L. Snelgrove, R.V. Strain, K.-H. Kim, J. Nucl. Mater. 304 (2002) 221.
[3] L. Lundberg, J. Nucl. Mater. 167 (1989) 64.
[4] H.J. Ryu, Y.S. Kim, G.L. Hofman, J. Nucl. Mater. 385 (2009) 623.
[5] M.E. Kassner, P.H. Adler, M.G. Adamson, D.E. Peterson, J. Nucl. Mater. 167 (1989) 160.
[6] S. Van den Berghe, W. Van Renterghem, A. Leenaers, J. Nucl. Mater. 375 (2008) 340.
[7] M.S. Daw, M.I. Baskes, Phys. Rev. B 29 (1984) 5;
M.W. Finnis, J.E. Sinclair, Philos. Mag. A 50 (1984) 6443.
[8] Ping Qian, Wei Su, Jiang Shen, Nan-Xian Chen, Comput. Mater. Sci. 43 (2008) 319.
[9] http://cst-www.nrl.navy.mil/lattice/index.html.
[10] O. Tougait, H. Noël, Intermetallics 12 (2004) 219.
[11] R. Zope, Y. Mishin, Phys. Rev. B 68 (2003) 24102.
[12] J.H. Rose, J.R. Smith, F. Guinea, J. Ferrante, Phys. Rev. B 29 (1984) 2963.
[13] S.M. Foiles, M.I. Baskes, M.S. Daw, Phys. Rev. B 33 (1987) 7983.
[14] R.C. Pasianot, E.J. Savino, Phys. Rev. B 45 (1992) 12704.
[15] J.E. Garcés, A.C. Marino, G. Bozzolo, 24th International Meeting on RERTR, Bariloche, Argentina, 2002.
[16] P. Söderlind, Phys. Rev. B 66 (2002) 085113.
[17] C. Kittel, Introduction to Solid State Physics, Wiley Interscience, New York, 1986.
[18] Ullmaier, Landolt-Börnstein, New Series III/25, 1991.
[19] G. Neumann, C. Tuijn (Eds.), Self-Diffusion and Impurity Diffusion in Pure Metals: Handbook of Experimental Data, vol. 14, Pergamon, 2008, p. 333.
[20] <http://www.ctcms.nist.gov/potentials/>.
[21] A.R. Miedema, Z. Metallkd. 70 (1979) 345.
[22] P.R. Alonso, J.R. Fernández, P.H. Gargano, G.H. Rubiolo, Phys. B 404 (2009) 2851.
[23] A.T. Dinsdale, CALPHAD 15 (1991) 317.
[24] H.H. Chiswik, A.E. Dwight, L.T. Lloyd, M.V. Nevitt, S.T. Zegler, in: Proc. of the 2nd United Nation International Conference on the Peaceful Uses of Atomic Energy, United Nations, Geneva, 1958.
[25] C.S. Barett, M.H. Mueller, R.L. Hitterman, Phys. Rev. 129 (1963) 625.
[26] C. Taylor, Phys. Rev. B 77 (2008) 094119.
[27] B. Beeler, B. Good, S. Rashkeev, C. Deo, M. Baskes, M. Okuniewski, J. Phys.: Condens. Matter 22 (2010) 505703.
[28] S. Xiang, H. Huang, L.M. Hsiung, J. Nucl. Mater. 375 (2008) 113.
[29] H. Matter, J. Winter, W. Triftshäuser, J. Nucl. Mater. 66 (1979) 085113.
[30] G. Henkelman, G. Jóhannesson, H. Jónsson, Methods for finding saddle points and minimum energy paths, in: S.D. Schwartz (Ed.), Progress on Theoretical Chemistry and Physics, Kluwer Academic Publishers, 2000, pp. 269–300.
[31] M.I. Pascuet, J.R. Fernández, A.M. Monti, Forum 272 (2007) 51.
[32] M.I. Pascuet, N. Castin, L. Malerba, J. Nucl. Mater. 412 (2011) 106.
[33] N. Metropolis, A.W. Rosenbluth, M.N. Rosenbluth, A.H. Teller, E. Teller, J. Chem. Phys. 21 (1953) 1087.
[34] W. Young, E. Elcock, Proc. Phys. Soc. 89 (1966) 735.
[35] L.L. Seigle, A.J. Opinsky, Nucl. Sci. Eng. 2 (1957) 38.
[36] R. Resnick, L.L. Seigle, J. Nucl. Mater. 5 (1962) 5.
[37] S.J. Rothman, J.J. Hines, J. Gray, A.L. Harkness, J. Appl. Phys. 33 (1962) 2113.
[38] S.J. Rothman, B. Bastar, J.J. Hines, D. Rokop, Trans. AIME 236 (1966) 897.
[39] P.Ch Sahu, V. Chandra Shekar, Pramana, J. Phys. 54 (2000) 685.
[40] J.P. Itié, J. Staun Oldsen, L. Gerward, U. Benedict, J.C. Spirlet, Physica 139 & 140B (1986) 330.
[41] H. Mehrer, Diffusion in Solids: Fundamentals, Methods, Materials, Diffusion-Controlled Process, Springer, 2007. p. 170.
[42] Y. Adda, M. Beyeler, A. Kirianenko, B. Pernot, Mem. Sci. Rev. Metall. 57 (1960) 423.
[43] J.H. Buddery, M.E. Clark, R.J. Pearse, J.J. Stebbs, J. Nucl. Mater. 13 (1964) 169.
[44] R.J. Pearce, R.D. Giles, L.E. Tavender, J. Nucl. Mater. 24 (1967) 129.
[45] R.D. Bland, Electrochem. Tech. 6 (1968) 272.
[46] F. Thummler, H.E. Lilienthal, S. Nazare, Powder Metall. 12 (1969) 1.
[47] D. Subramanyam, M.R. Notis, J.I. Goldstein, Metall. Trans. A 16 (1985) 589.
[48] L.S. Castleman, J. Nucl. Mater. 3 (1961) 1.
[49] M.I. Mirandou, S.N. Balart, M. Ortiz, M.S. Granovsky, J. Nucl. Mater. 323 (2003) 29.
[50] A.D. Le Claire, I.J. Bear, J. Nucl. Energy 2 (1956) 229.
[51] E. Perez, B. Yao, Y.H. Sohn, D.D. Keiser Jr., in: Proceedings of the XXXI RERTR International Meeting, Beijing, China, November 1–5, 2009.